



Icaritin Enhancing Bone Formation Initiated by Sub-Microstructured Calcium Phosphate Ceramic for Critical Size Defect Repair

Haitao Peng^{1†}, Jianxiao Li^{2†}, Yanan Xu³ and Guoyu Lv^{1*}

¹College of Physics, Sichuan University, Chengdu, China, ²Department of Orthopedics, The First Affiliated Hospital of Chongqing Medical University, Chongqing, China, ³Department of Trauma Surgery, Emergency Medical Center of Chongqing, Chongqing, China

OPEN ACCESS

Edited by:

Gang Wu,
VU University Amsterdam,
Netherlands

Reviewed by:

Janos Kanczler,
University of Southampton,
United Kingdom
Dongxia Ye,
University of Rochester, United States

*Correspondence:

Guoyu Lv
lgy929@126.com

[†]These authors have contributed
equally to this work

Specialty section:

This article was submitted
to Biomaterials,
a section of the journal
Frontiers in Materials

Received: 23 August 2020

Accepted: 30 October 2020

Published: 11 December 2020

Citation:

Peng H, Li J, Xu Y and Lv G (2020)
Icaritin Enhancing Bone Formation
Initiated by Sub-Microstructured
Calcium Phosphate Ceramic for
Critical Size Defect Repair.
Front. Mater. 7:598057.
doi: 10.3389/fmats.2020.598057

Adequate bone tissue regeneration has been challenging to achieve at critical-sized bone defects caused by disease. Bone tissue engineering using a combination of scaffolds and bioactive factors provides new hope for the treatment of this extreme condition. Icaritin, a herb-derived chemical, has shown its ability to enhance bone formation both *in vitro* and *in vivo*, and it has been found that sub-micron surface structure instructs bone formation in calcium phosphate ceramics (CaPs). Here, we evaluated the possibility of using a submicron surface structured CaP ceramic as the carrier of icaritin for bone tissue regeneration in critical-sized bone defects. Icaritin, an herb-derived chemical, was loaded into a submicron surface structured porous calcium phosphate ceramic ($\text{Ø}12.8 \times 3 \text{ mm}$) to get samples with 0, 10, 50, 250, and 1,250 μg icaritin per CaP disc (M0, M10, M50, M250, M1250 groups, respectively). *In vitro* evaluation with the certain dosages correlated to those released from the samples showed a dose-dependent enhancement of osteogenic differentiation and mineralization of human bone marrow stromal cells with the presence of osteogenic factors in the culture medium, indicating icaritin is an osteopromotive factor. After intramuscular implantation of the samples in dogs for 8 weeks, a dose-dependent of bone formation was seen with enhanced bone formation at the dosage of 50 and 250 μg . To evaluate the *in vivo* osteogenic potentials of icaritin-containing CaP ceramic scaffolds in the orthopedic site, a 12.8 mm calvarial defect model in rabbits was established. Micro-computed tomography (micro-CT) and histology results at weeks 4, 8 and 12 post-surgery showed more newly formed bone in M250 group, with correspondingly more new vessel ingrowth. The results presented herein suggested that being osteopromotive, icaritin could enhance bone formation initiated by sub-microstructured CaP ceramics and the CaP ceramics scaffold incorporating icaritin is a promising biomaterial for the treatment of critical-sized defect.

Keywords: icaritin, submicron surface structure, calcium phosphate ceramic, critical-sized bone defect, bone regeneration

INTRODUCTION

The orthopedic critical-sized defect due to traumatic injuries or tumor resection is still a significant challenge. Pursuing alternatives to autologous bone grafts has always been a goal of biomaterial engineering. Allowing bone formation on their surface and form chemical bonding to the new bone, calcium phosphate (CaP) ceramics have been widely used as bone graft substitutes (Hench and Wilson, 1984; Damien and Parsons, 1991; Bohner et al., 2012). However, compared with autogenous bone, the capacity of CaP ceramics for repairing critical-sized defects still seems to be insufficient.

Surface modification may improve the bone regeneration ability of CaP ceramics. When the surface structure of CaP ceramics decreased from micron to submicron scale, it induced bone formation in the muscle of dogs (Davison et al., 2014b; Zhang et al., 2014) and under the skin of FVB mouse (Davison et al., 2014a). Having the osteoinductive property, calcium phosphate ceramics not only enhanced bone regeneration in non-critically sized bone defects (Habibovic et al., 2004; Yuan et al., 2006) but also could repair critical-sized defects (Yuan et al., 2010) and enhance bone formation in the spinal environment (van Dijk et al., 2018).

Besides, osteogenic factors can also exert considerable bone repair effects when combined with scaffolds (McMillan et al., 2018). Icaritin, an exogenous semi-synthesized small phytomolecule, is an intestinal metabolite of herbal epimedium-derived flavonoids (Zhang et al., 2007; Qin et al., 2008), and has shown to affect various biological processes. For instance, it inhibited both thrombosis and lipid-deposition reducing thus the incidence of steroid-associated osteonecrosis (Zhang et al., 2009), and it exhibited *in vitro* anti-inflammatory effects on the mouse peritoneal macrophages (Lai et al., 2013). Most recently, the roles of icaritin in bone metabolism were also found. It enhanced the differentiation and proliferation of osteoblasts, facilitated matrix calcification (Qin et al., 2008; Yao et al., 2012), and enhanced bone regeneration in an ovariectomized rat osseous model (Zhang et al., 2008; Peng et al., 2013).

Although icaritin exhibits bone-enhancing effects in PLGA/TCP scaffolds (Chen et al., 2012; Chen et al., 2013), there is no report on the combination of icaritin and inorganic ceramics to repair the critical-sized defect. More notably, when icaritin was loaded on a special submicron structured CaP scaffold, it is unknown whether the bone regeneration ability of CaP ceramics is enhanced.

We hypothesized that the combination of chemicals enhancing bone formation and osteoinductive calcium phosphate ceramics would result in bone substitutes with improved bone regeneration capacity for critical-sized defect repair. Considering the possible bone-enhancing function of icaritin as previously shown, we introduced icaritin into sub-micron surface structured tricalcium phosphate ceramic and characterized the resulting materials concerning for their physicochemical properties and icaritin release. Following the *in vitro* evaluation of icaritin released with hBMSCs, we investigated the bone-forming ability of the materials after

intramuscular implantation in a canine model. According to previous research, rabbit calvarial defect is a mature model for evaluating the bone reparability of biological scaffolds, but the critical defect size rarely exceeds 10 mm (Xu et al., 2008; Lee et al., 2018). In this study, we designed a 12.8 mm critical bone defect to investigate the bone repair effect of the materials by micro-computed tomography (micro-CT) and histology. With results showing, the sub-microstructured CaP ceramics scaffold incorporating icaritin could be a promising biomaterial for the treatment of critical-sized defect.

MATERIALS AND METHODS

Preparation and Physico-chemical Properties of CaP Ceramics With Sub-micron Scale Surface Structure

CaP powder was synthesized by neutralization reaction method at Ca/P ratio of 1.5. H_3PO_4 solution was dropped into a $Ca(OH)_2$ suspension to get CaP powder. The porous CaP green bodies were obtained using H_2O_2 (1%) and wax particles and then sintered at $1,050^\circ C$ for 8 h to form ceramics (Yuan et al., 2010; Zhang et al., 2014; Zhang et al., 2015). Microporous discs ($\varnothing 12.8 \times 3$ mm) were machined from the ceramic bodies using a lathe and a diamond saw microtome (Leica SP1600). Discs were ultrasonically cleaned in successive baths of acetone, ethanol, and deionized water, and then dried at $60^\circ C$.

X-ray diffraction (XRD; Rigaku, Tokyo, Japan) was used to analyze the crystal structure of CaP powder. The grain, micropore size and surface topography was detected by scanning electron microscope (XL30, ESEM-FEG, Philips, Eindhoven, The Netherlands). Especially, the grain and micropore was selected randomly from the image and the vertical lengths crossing the center of each grain and micropore were considered to be the grain and pore size. Mercury intrusion was used to obtain the ceramics' total porosity, microporosity and micropore size distribution.

In vitro Release of Icaritin by CaP Scaffold in Calcium Medium

CaP discs were sterilized with autoclave at $121^\circ C$ for 30 min. Icaritin solutions of 0, 40, 200, 1 and 5 mg/ml were prepared with methyl alcohol and sterilized with $0.2 \mu m$ filter (Acrodisc[®] 13 CR PTFE $0.2 \mu m$, Gelman Pall). Under sterile condition, $250 \mu L$ of each icaritin solution was loaded onto CaP disc. Thereafter, methyl alcohol was evaporated in sterile conditions at $50^\circ C$ with ventilation for seven days to obtain samples containing 0 μg icaritin per disc (M0), 10 μg icaritin per disc (M10), 50 μg icaritin per disc (M50), 250 μg icaritin per disc (M250) and 1,250 μg icaritin per disc (M1250) respectively. Then, samples ($n = 3$) were individually incubated in 3 ml of culture medium containing *a*-MEM (Lonza), 10% FBS (Gibco) and 1% antibiotics (100 U/ml penicillin and 100 $\mu g/ml$ streptomycin, Invitrogen) at $37^\circ C$ and 5% CO_2 . Culture medium was refreshed at day 1, 2, 4, 7, 14, 21, 28, 35, 42, 49 and day 56 respectively. The medium

collected at each refreshment point were stored at -20°C before further use.

Icaritin concentration in medium was detected with an HPLC-MS/MS system (TSQ Quantum Ultra, ThermoFisher Scientific, Co. Ltd., USA) equipped with a surveyor Autosampler, a mass pump and a triple quadrupole mass spectrometer. Six standard icaritin solutions in culture medium (i.e., 2, 5, 50, 100, 250, and 500 ng/ml) were prepared for a calibration line. The icaritin concentration in the samples was calculated according to the calibration line, while the remaining icaritin was calculated by subtracting the cumulative icaritin release from the original loading.

To determine the solubility of icaritin in water and culture medium, icaritin was directly added to water and culture medium at 37°C overnight and centrifuged at 5,000 rpm for 5 min. The supernatants ($n = 3$) were subjected to HPLC-MS/MS assay.

***In vitro* Evaluation With Human Bone Marrow Stromal cells (hBMSC) Medium Preparation**

Basic medium (BM), Growth medium (GM) and Osteogenic medium (OM) were used in the *in vitro* cell culture. Basic medium was α -MEM (Invitrogen, United Kingdom) supplemented with 10% FBS (Lonza, Germany), 2 mM L-Glutamine (Invitrogen, United Kingdom), 0.2 mM L-Ascorbic acid 2-phosphate (AsAP, Sigma), 100 IU/ml penicillin (Invitrogen, United Kingdom) and 100 g/ml streptomycin (Invitrogen, United Kingdom), growth medium was basic medium supplemented with 1 ng/ml basic fibroblasts growth factors (bFGF, Instruchemie, the The Netherlands), and osteogenic medium was basic medium supplemented with 10 nM dexamethasone (Sigma) and 10 mM-glycerophosphate (Sigma) (Luo et al., 2014).

Icaritin was added to BM and OM according to the saturated concentration of icaritin in culture medium with/without the presence of CaP ceramic discs (e.g., 2,000 and 4,300 ng/ml, as obtained from icaritin release test), thus both BM and OM containing 0, 20, 200, 2,000 and 4,300 ng/ml icaritin were prepared by first dissolving 5 mg icaritin in 10 ml methyl alcohol as the stock solution, followed by diluting this stock solution with either BM or OM. Specifically, additional methyl alcohol was added to each medium to keep the methyl alcohol concentration in all medium consistent.

Human Bone Marrow Stromal Cells (hBMSC) Cultivation

hBMSc (Passage 3, D307, Lonza) were expanded in cell culture flasks with GM under a humidified atmosphere of 5% CO_2 at 37°C until 80% confluence. Then GM was removed, and cells were harvested with 0.25% trypsin (Invitrogen, United Kingdom). 5,000 cells/well were seeded in 48-well cell culture plates ($n = 5$ per condition at each time point) and cultured with various medium prepared as described above. The medium was refreshed twice a week accordingly, and cells were harvested after 1, 4, 7, 14, and 21 days for further assays.

Cell Morphology

By day 14, cells were rinsed once with 37°C phosphate-buffered saline (PBS) and fixed with 4% formaldehyde solution at room temperature for 10 min. Afterwards, the fixation solution was removed and cells were rinsed again with PBS and stained with 1% methylene blue solution for 1 min. Cell morphology was visualized using a Nikon SMZ800 stereomicroscope equipped with a Nikon camera.

Calcium Deposition

By day 14, 21, cells were rinsed once with 37°C phosphate-buffered saline (PBS) and fixed with 4% formaldehyde solution at room temperature for 10 min. Afterwards, the fixation solution was removed, and cells were rinsed once with PBS, twice with distilled water and stained with 2% alizarin red staining for 1 min. Excessive staining was rinsed twice with distilled water. Staining was visualized using a Nikon SMZ800 stereomicroscope equipped with a Nikon camera.

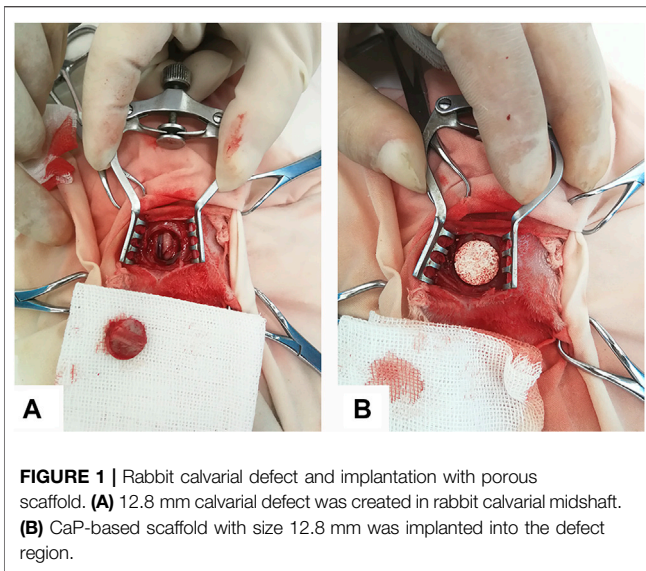
Cell Proliferation and Osteogenic Differentiation Assay

By day 1,4,7,14,21, cells were frozen at -80°C for 24 h after rinsed once with 37°C phosphate-buffered saline (PBS). The proliferation of hBMSCs was analyzed with a CyQuant cell proliferation assay kit (Invitrogen). Briefly, to obtain the cell lysate, 150 μL CyQuant lysis buffer was added to each well after cell culture plates were thawed at room temperature, followed by shaking at 400 rpm for 5 min. Then GR reagent was diluted 400 times by CyQuant lysis buffer. After 100 μL diluted reagent was incubated with 100 μL cell lysate for 5 min in the dark at room temperature, the fluorescence was detected using a spectrophotometer (Anthos Zenyth 3100) at wavelength of 480 nm for excitation and 520 nm for emission.

By using AttoPhos[®] AP fluorescent substrate system (catalog S1000, Promega), the amount of 2-[2-benzothiazoyl]-6-hydroxybenzothiazole (BBT) produced during the reaction was used to present the Alkaline phosphatase (ALP) activity. Briefly, 90 μL substrate reagent was incubated with 10 μL cell lysate for 15 min in dark at room temperature. The fluorescence signal was then collected using a spectrophotometer (Anthos Zenyth 3100).

Ectopic Implantation

To study the influence of icaritin on bone formation, the icaritin-CaP discs (M0, M10, M50, M250, M1250) were evaluated in canine and rabbit ectopic models. All the animal experiments were followed the "Guidance Suggestions for the Care and Use of Laboratory Animals" by the National Science and Technology Committee of the People's Republic of China in order No. 2, 2006. Icaritin-CaP discs were implanted in the para-spinal muscles of five adult male beagles (body weight 14–17 kg) for 8 weeks. The surgeries were performed under general anesthesia by abdominal injection of sodium pentobarbital (30 mg/kg body weight) under sterile conditions. Following the surgeries, penicillin (40 mg/kg body weight) was injected intramuscularly for three consecutive days to prevent infection. After operation, all animals were allowed to bear full weight and received a normal diet.



The animals were sacrificed via celiac injection of an excessive amount of pentobarbital sodium at week 8. Implants were harvested with the surrounding tissues and fixed in 4% formaldehyde at 4°C for 1 week.

Calvarial Defect Repair Surgery

Thirty-six adult male New Zealand white rabbits (body weight 2.8–3.0 kg) were used for this study. According to the results of **Section 2.4**, thirty-six rabbits were divided into two groups with M0 as the control group and M250 as the experimental group. All the animal experiments were followed the “Guidance Suggestions for the Care and Use of Laboratory Animals” by the National Science and Technology Committee of the People’s Republic of China in order No. 2, 2006. The surgeries were performed under general anesthesia by abdominal injection of sodium pentobarbital (30 mg/kg body weight) under sterile conditions. After proper preparation, a midline sagittal incision in the scalp was made to expose the parietal bone and a critical-size (12.8 mm in diameter) defect was created in the middle of parietal bone using a sterile drill (**Figure 1A**). After the bone was removed, the defects were grafted with porous icaritin-CaP ceramics (**Figure 1B**) and the incision was closed in layers using 4–0 Vicryl sutures. Following the surgeries, penicillin (40 mg/kg body weight) was injected intramuscularly for three consecutive days to prevent infection. After operation, all animals were allowed to bear full weight and received a normal diet.

At week 4, week 8, and week 12, each group of experimental animals was divided into an ink injection group and a non-ink injection group, with 3 animals in each group. To observe the growth of blood vessels, the animals in the ink injection group were injected with ink diluted with physiological saline (ratio 1:4) at a dose of 40 ml/kg after semi-anaesthesia with barbiturate sodium. The non-ink injection group was killed with an excess of pentobarbital sodium. All the defects with an additional 2 mm surrounding tissue were dissected from the host bone.

The samples of the ink injection group were fixed in 4% formaldehyde for histological quantification. After each sample in the non-ink injection group was divided into two halves, half was stored in liquid nitrogen for genetic testing, the other half was fixed in 4% formalin for histological observations.

Quantitative Reverse Transcription-PCR (qRT-PCR)

VEGF and FGF are crucial factors in angiogenesis. To determine the VEGF- and FGF-promoting effects of icaritin, qRT-PCR analyses were performed. All the samples were lysed in Trizol reagent (Ambion, USA), total RNA was extracted following the manufacturer’s protocol (Chengdu Lilai Technology Co. Ltd., China) and reverse transcription was performed using RevertAid First Strand cDNA Synthesis Kit (Thermo Fisher Scientific, USA). Gene expressions were quantified using SYBR Green I PCR Kit (FastStart universal SYBR Green Master (Rox); Roche, Switzerland) in Real-Time PCR System (Thermo Fisher Scientific, USA). β -Actin was used as the housekeeping gene. Primers of the target genes including VEGF and FGF were listed in **Table 1**. Finally, the Real-time PCR reactin was run at 95 for 10 min, followed by 95 for 30 s, 55 for 30 s and 72 for 30 s for 45 cycles. The data were analysed using Thermo Scientific PikoReal software. The relative amounts of target genes normalized by β -Actin were calculated by the $2^{-\Delta CT}$ method, where $\Delta C_T = C_{T, target} - C_{T, \beta-Actin}$.

Micro-CT

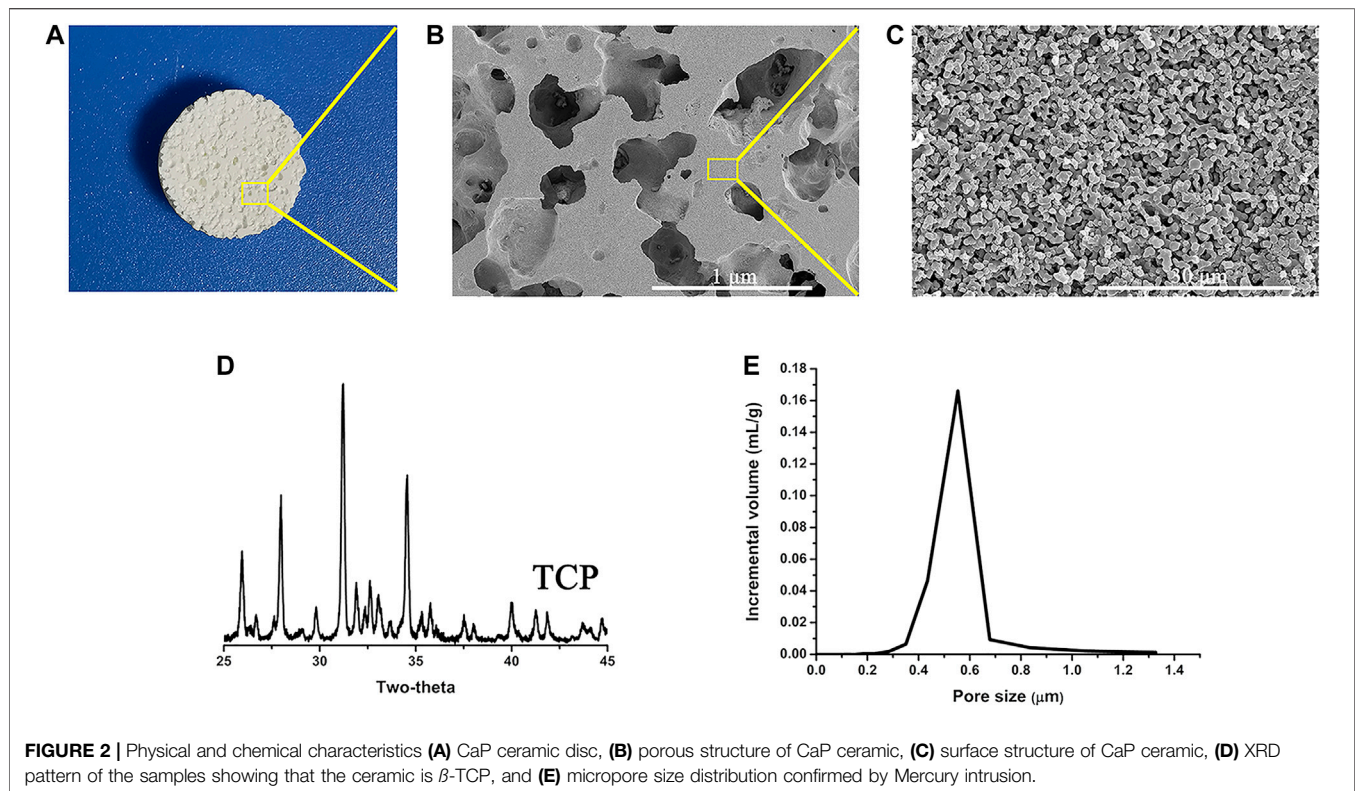
Micro-CT (medium-resolution mode, isotropic voxel size: 15 μ m; mCT 80, Scanco Medical AG, Bassersdorf, Switzerland) was used to evaluate new bone formation within the implants. The horizontal plane of all samples must be oriented perpendicular to the axis of the X-ray beam. The 2D radiographic images were used to reconstruct and calculate corresponding bone volume fraction (bone volume/total volume, BV/TV) with Scanco software by thresholding ($n = 3$) (Chai et al., 2012; Ji et al., 2020).

Histological Observations

After fixation, all the harvested samples were dehydrated through a series of increasing ethanol concentrations and were subsequently embedded in methylmethacrylate. Three non-decalcified sections (10–20 μ m) from mid-defect regions of each sample were made by using a diamond saw microtome (Leica SP-1600, Germany) and stained with 1% methylene blue (Sigma) and 0.3% basic fuchsin (Sigma) solutions for qualitative and quantitative histological observations.

TABLE 1 | Primer sequences for RT-PCR.

Gene	Primer sequences (5’–3’)	
	Sense	Antisense
β -Actin	GCTTCTAGGGGACTGTTAG	CGAATAAAGCCATGCCAATCTC
VEGF	TGGCAGAAGAAGGAGACAATAAA	GAAGATGTCCACCAAGGTCTC
FGF	GCGACCCACACATCAAATTAC	GCAGTCTTCCATCTTCTTCA



To perform histomorphometry, the histological slides were scanned (Dimage Scan Elite 5400II, Konica Minolta photo Imaging Inc., Tokyo, Japan). After that, using Adobe Photoshop CS5 software, the region of interest (ROI), the ceramic materials (M) and bone (B) were quantified as the pixel values. Bone formation in the available space was quantitatively determined as follows: $B\% = B \cdot 100 / (ROI - M)$. Qualitative histology analysis of tissue formation (i.e. cell type, bone formation and presence of blood vessels) was performed by observing the slides at the light microscope (Nikon Eclipse E200, Tokyo, Japan).

STATISTICS

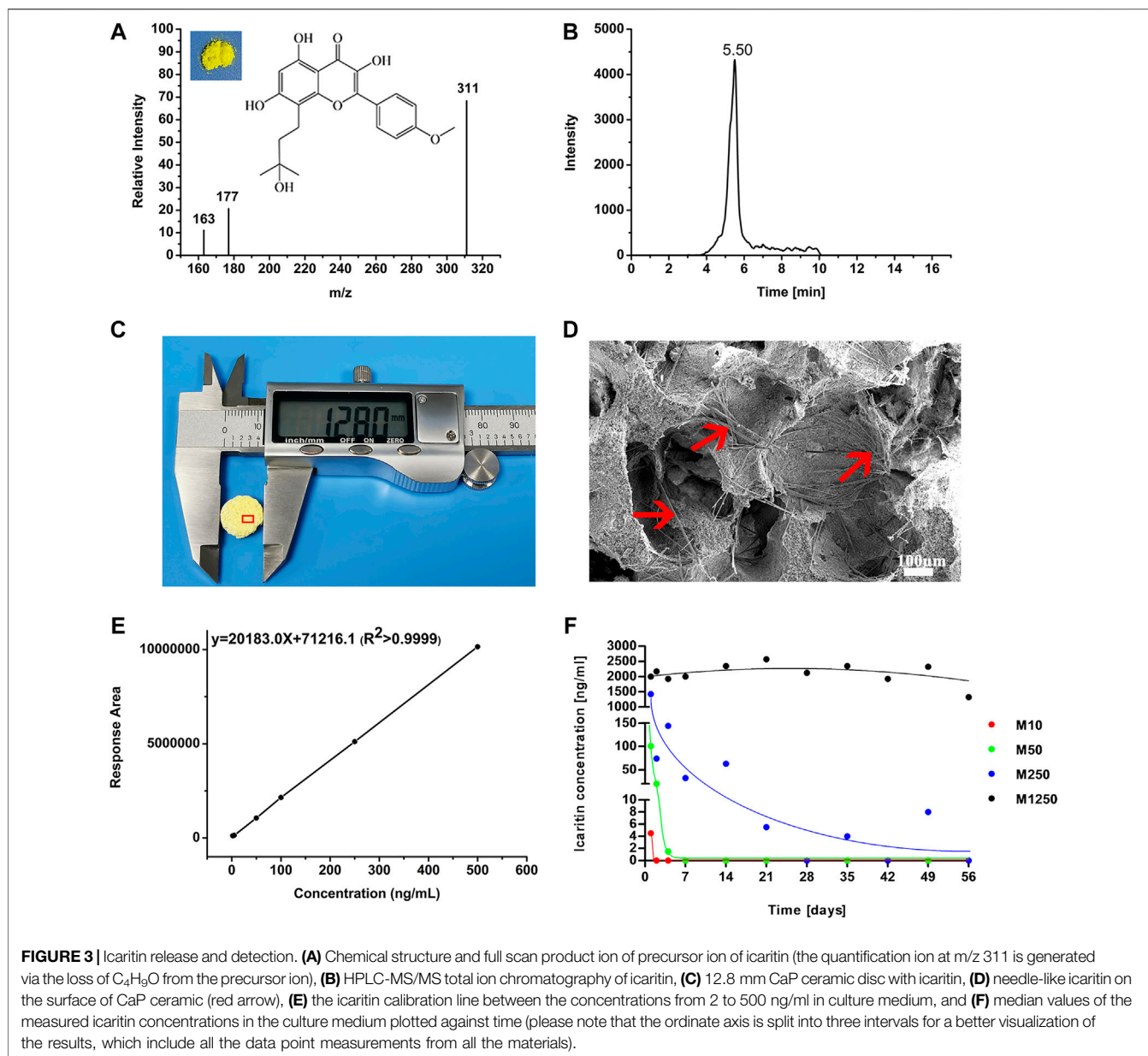
During the icaritin release experiment, multiple measures were performed on each sample, thus median of the measured data was used to reduce the effects of outliers. Mean was considered to represent bone formation as the sample number was limited. In the experiment of icaritin release, the data points were fitted with non-linear regression models to study the trend during time and were compared using one-way Wilcoxon signed rank-sum test. When means were considered, multiple comparisons were performed with one-way analysis of variance (ANOVA) followed by Bonferroni post-test comparisons. p -values lower than 0.05 were considered as statistically significant differences.

RESULTS AND DISCUSSION

The CaP Ceramic Scaffold and Release Characteristics

Figure 2B shows the porous structure of CaP ceramic, and the XRD pattern of CaP indicates that the ceramic is β -TCP (**Figure 2D**). Observing the microstructure size by SEM, CaP ceramic has a grain size of $0.95 \pm 0.20 \mu\text{m}$ and a micropore size of $0.65 \pm 0.25 \mu\text{m}$ (**Figure 2C**). Mercury intrusion indicates that the ceramic micropores range from 0.2–1.3 μm with a peak of 0.55 μm (**Figure 2E**). It can be seen from the Mercury intrusion data that the total porosity is 62% and the microporosity is 23%.

Icaritin crystals could be observed on the surface of CaP ceramic and are rod-like with a diameter smaller than 10 μm (**Figures 3C,D**). To detect icaritin with the HPLC-MS/MS system, optimization of precursor and product ions of the icaritin for MRM analysis by a triple quadrupole mass spectrometer with electrospray ionization was performed. The m/z response observed was much better in the negative ionization mode than in the positive mode due to the phenolic hydroxyl group. The mass spectra showed deprotonated molecular ion $[M-H]^-$ peak at 385.0 m/z . On the basis of the production mass spectra, the major fragment ion was observed at 311.1 for icaritin (**Figure 3A**). A total ion chromatogram in full scan model was generated using standard icaritin solution, and icaritin could be separated and eluted at 5.50 min (**Figure 3B**). A good linearity was obtained for icaritin over the range from 2 to 500 ng/ml in culture medium (**Figure 3E**).



According to the calibration line, the saturated icaritin concentrations at 37°C were $13.4 \pm 2.4 \mu\text{g/ml}$ in water and $4.3 \pm 0.1 \mu\text{g/ml}$ in culture medium respectively. The release of icaritin from the samples is summarized in **Table 2** and illustrated in **Figure 3F**. No icaritin was detected in any of the controls (group M0). Initial burst releases, directly correlated with the icaritin content in the discs, were observed on the first day for all those samples containing icaritin (**Figure 3F**): the lesser icaritin incorporated in the CaP ceramic, the minor the intensity of the burst. Afterwards, all materials but M1250 had exponential release decays. The samples with the smaller icaritin amount M10 ceased to release already on the second day of experiment. A similar but delayed trend was observed for those samples containing 50 μg of icaritin, which stopped releasing after one week. Discs with an initial load of 250 μg icaritin were able to have

TABLE 2 | The quantities of total (cumulative) released and remaining icaritin in the samples after 56 days soaking.

Sample	Total icaritin released after 56 days (μg)	Percentage of released icaritin
M0	0	0
M10	0.052 ± 0.065	0.52%
M50	0.37 ± 0.06	0.74%
M250	5.54 ± 0.58	2.21%
M1250	69.80 ± 11.91	5.58%

a significant longer release decay rate as compared to M10 and M50. Samples M1250, with the highest icaritin initial content, kept a steady release during the whole experiment. The four materials, until they released icaritin, had significantly different

release trends ($p < 0.05$ for all data sets when compared in the periods of active release). The release measurements were corroborated by the observation that the majority of icaritin stayed in the discs after a 56-days soaking in culture medium (Table 2).

By its chemical nature, icaritin is theoretically not soluble in aqueous solution, and a low solubility of icaritin was seen in the study. In water, a saturated concentration of $13.4 \pm 2.4 \mu\text{g/ml}$ was reached at 37°C . The saturated concentration decreased to $4.3 \pm 0.1 \mu\text{g/ml}$ in the simulated body fluids (eg Dulbecco's Modified Eagle Medium plus foetal bovine serum), agreeing with the influence of proteins and ions on the solubility of chemicals (Galia et al., 1998). With a low solubility, a sustained release of icaritin was expected when it was loaded onto carriers. The sustained release was achieved in practice at the highest dose used in the study (e.g., M1250). The release profile of icaritin (Figure 3F and Table 2) indicated that icaritin was not only physically loaded into the CaP ceramic but also reacted chemically to CaP. If only physical loading was there, the constant release of icaritin from M1250 should be around $4.3 \mu\text{g/ml}$ in simulated body fluids, while it was $2.0 \mu\text{g/ml}$ in practice. Moreover, if only physical loading was there, a constant release could have happened in the case of $250 \mu\text{g}$ icaritin/disc as well, since the total theoretical release of icaritin in the tested time frame was $141.9 \mu\text{g}$ (11-time points with the theoretical constant release of $4.3 \mu\text{g/ml}$ in 3 ml), less than $250 \mu\text{g}$ icaritin loaded. As shown in Table 2, the majority of icaritin was retained in CaP ceramics after a 56-days soaking in simulated body fluids, further supporting the chemical reaction of icaritin to the CaP ceramic. The exact reaction of icaritin to CaP ceramic needs to be further addressed with studies, while it is likely that icaritin could react to calcium phosphate through coordination bond with Ca^{2+} ions, meaning that there might exist some dynamic equilibria involving icaritin and Ca^{2+} ions (Huskens and Sherry, 1998). As such, the saturated concentration of icaritin further decreased to $2.0 \mu\text{g/ml}$ in simulated body fluids when loaded into the CaP ceramic (Figure 3F, M1250).

Influence of Icaritin on hBMSCs

Bearing the possible reaction between icaritin and CaP ceramic after loading, icaritin released from CaP ceramic discs into simulated body fluids dose-dependently (Figure 3F). Using the saturated concentration in culture medium and dilutions of the highest icaritin release from CaP ceramic into culture medium (e.g., $2 \mu\text{g/ml}$), the influence of icaritin on the activities of human bone marrow stromal cells was evaluated. A morphological change from spindle to polygon shape was observed by day 14 with the increasing concentration of icaritin (Figure 4B), regardless of the culture media used (BM vs OM). Specifically, with the increasing of icaritin up to $2,000 \text{ ng/ml}$, hBMSCs became more spread and larger, indicating their tailored cell fate in the presence of icaritin. In both BM and OM $2,000 \text{ ng/ml}$ icaritin inhibited the proliferation of hBMSCs while $4,300 \text{ ng/ml}$ icaritin showed severe cytotoxicity that it induced apoptosis, where not much cells but crystals of un-dissolved icaritin were observed

under the light microscope instead of living cells (Figure 4B, $4,300 \text{ ng/ml}$).

Calcium deposition was only observed in OM group but not in BM (Figure 4A). By day 14 and 21 the calcium deposition was seen in 20 ng/ml and 200 ng/ml , and occasionally seen in $2,000 \text{ ng/ml}$ and $4,300 \text{ ng/ml}$.

hBMSCs proliferated and peaked by day 14 in both BM and OM, except in those supplemented with 2000 ng/ml icaritin or more (Figure 4D). With the presence of osteogenic factor (e.g., DEX), cells, in the means of DNA content, were not much different in number among the groups of 0, 20, and 200 ng/ml , while without osteogenic factor, cells were much more in number in groups of 20 and 200 ng/ml as compared to 0 ng/ml control (Figure 4D).

Given the fact that a high dose of icaritin was harmful to the cells, ALP assay was not applied to the samples of $4,300 \text{ ng/ml}$ icaritin/ml. The ALP expression of hBMSCs is relatively low in BM as compared to OM group regardless of the concentration of icaritin (Figure 4C). Moreover, ALP/DNA in cells cultured with BM did not increase with time from Day 7 to Day 21, while ALP/DNA increased from Day 7 to Day 21 (Figure 4C) in cells cultured with OM. Furthermore, at day 21, ALP/DNA was up to the concentration of icaritin, with higher ALP/DNA at higher concentration of icaritin (at the dose range of $0\text{--}200 \text{ ng/ml}$) (Figure 4C).

So, at the saturated concentration in culture medium ($4.3 \mu\text{g/ml}$), icaritin was harmful to hBMSCs and caused cell death (Figures 4B,D). At the highest release from CaP ceramic ($2 \mu\text{g/ml}$ from M1250), icaritin inhibited cell proliferation (Figures 3B, 4D). At the concentration between $0.02\text{--}0.20 \mu\text{g/ml}$, icaritin enhanced proliferation of hBMSCs in the absence of osteogenic factor (eg Dex), while it did not affect hBMSC proliferation when dex was used in the culture media (Figures 4B,D). At the concentration of $0.02\text{--}0.20 \mu\text{g/ml}$, icaritin did not enhance osteogenic differentiation of hBMSCs when Dex was not used in the culture medium, as indicated in both mineralization assay (Figure 4A) and ALP/DNA assay (Figure 4C), with the presence of Dex in the culture media, icaritin did enhance osteogenic differentiation of hBMSCs (Figures 4A,C). The data agreed with the previous findings that at certain dosages icaritin did not affect bone marrow stromal cell proliferation, but enhanced ALP production and mineralization while at high doses, meaning that icaritin enhances osteogenic function of readily differentiated osteogenic cells but does not induce osteogenic differentiation of osteoprogenitors or stems cells *in vitro*.

Influence of Icaritin in Ectopic Bone Formation

When icaritin-loaded CaP ceramic discs were implanted intramuscularly in canine for 8 weeks, the dose-dependent influence of icaritin on bone formation was seen (Figures 5, 6). The samples ($n = 5$) harvested from all animals were available for histological evaluation and histomorphometry. The least bone formation was observed in group M1250 and most bone formation occurred in groups M50 and M250 (Figures 5, 6).

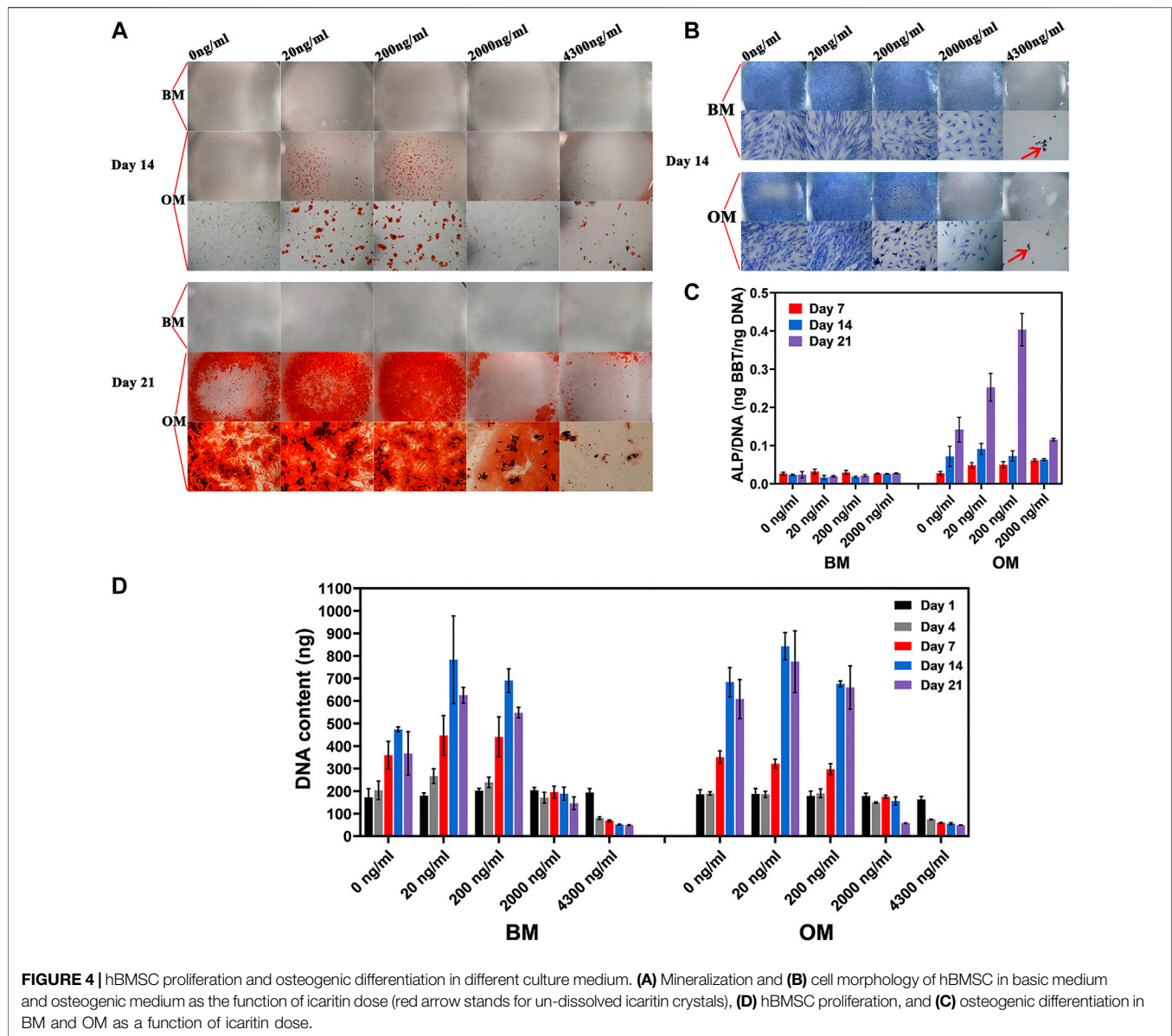


FIGURE 4 | hBMSC proliferation and osteogenic differentiation in different culture medium. **(A)** Mineralization and **(B)** cell morphology of hBMSC in basic medium and osteogenic medium as the function of icaritin dose (red arrow stands for un-dissolved icaritin crystals), **(D)** hBMSC proliferation, and **(C)** osteogenic differentiation in BM and OM as a function of icaritin dose.

The addition of 10 μg did not improve bone formation as compared to the control group. Loading 50 or 250 μg icaritin significantly increased the bone formation in the CaP ceramic. When icaritin was added in a high dose (i.e., 1,250 μg), it had an inhibitory effect on the ectopic bone formation of the ceramic.

Both the icaritin liberated from CaP ceramic and the icaritin that stayed in the CaP ceramic may have played biological roles *in vivo*. At the concentrations of 10^{-7} – 10^{-5} mol/L (i.e., 0.0385–3.85 $\mu\text{g}/\text{ml}$), icaritin enhanced the differentiation and proliferation of osteoblasts *in vitro* (Huang et al., 2007). If only the icaritin liberated from CaP ceramic affected bone formation, then bone formation may not have been enhanced in the 50 μg icaritin group since the release of icaritin stopped 7 days after immersing in simulated body fluid, while it was known that inductive bone formation in canine muscle normally starts

4 weeks after implantation (Yuan et al., 2006). Similarly, if only the icaritin released from CaP ceramic had an essential contribution, then bone formation should have been enhanced in the 1,250 μg group in dogs because the 2 $\mu\text{g}/\text{ml}$ concentration was still within the reported interval of efficient icaritin concentration to enhance bone formation. Instead, it was found in this study that the bone formation was inhibited in the 1,250 μg group. The inhibited bone formation in the 1,250 μg group could be attributed to the cytotoxicity of icaritin at high dosages (Chen et al., 2012; Chen et al., 2013).

Based on the *in vitro* results, it is clear that icaritin does not have osteoinductive potential as the bone morphogenetic proteins have (Chen et al., 2012), icaritin could thus only affect bone formation in an environment where bone formation was readily present. In other words, icaritin enhanced a bone formation process that was already triggered by the submicron scaled

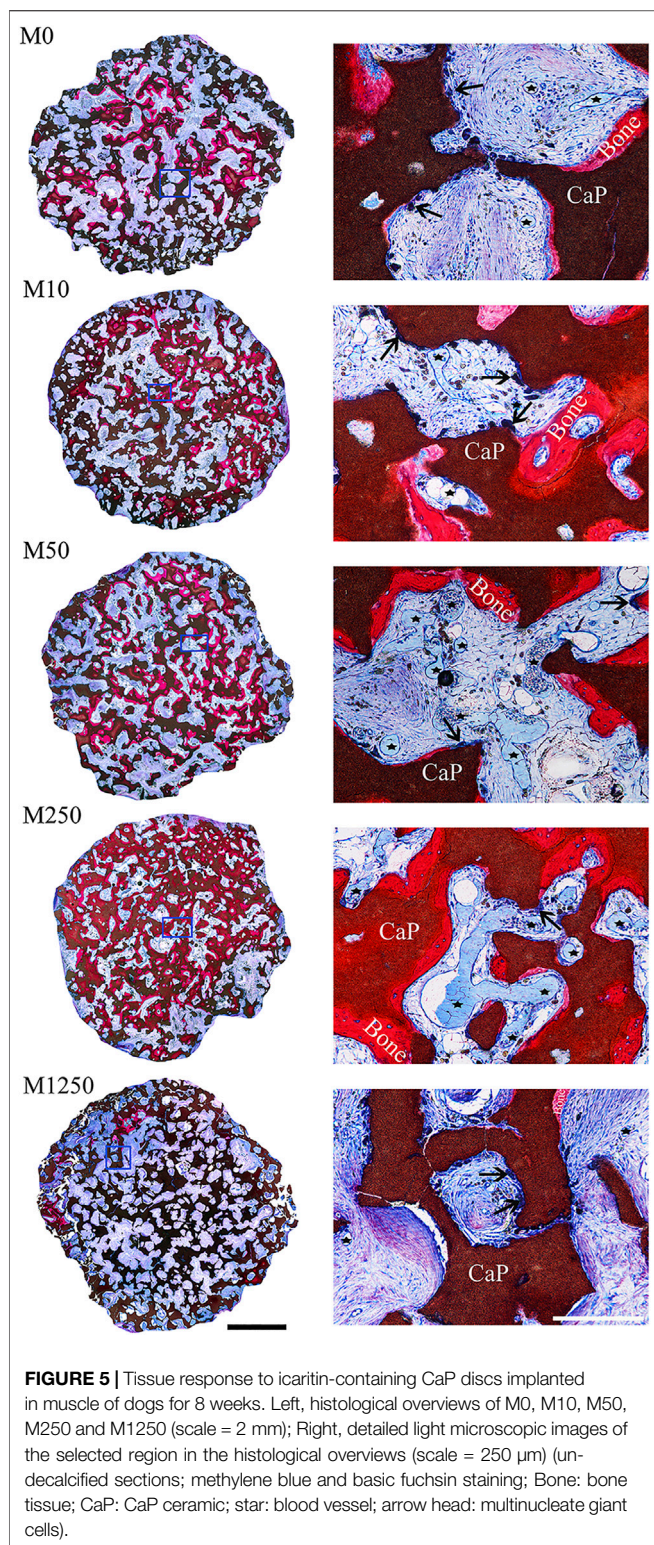


FIGURE 5 | Tissue response to icaritin-containing CaP discs implanted in muscle of dogs for 8 weeks. Left, histological overviews of M0, M10, M50, M250 and M1250 (scale = 2 mm); Right, detailed light microscopic images of the selected region in the histological overviews (scale = 250 μm) (undecalcified sections; methylene blue and basic fuchsin staining; Bone: bone tissue; CaP: CaP ceramic; star: blood vessel; arrow head: multinucleate giant cells).

surfaces of the CaP ceramic implanted in this study in dogs. Via protein adsorption (Yuan et al., 2010; Zhang et al., 2014), surface mineralization (Zhang et al., 2015; Murr, 2019), ion-release (Yuan et al., 2010; Zhang et al., 2014; Zhang et al., 2015) and surface topographic cues (Zhang et al., 2015), submicron surface

structured calcium phosphate ceramic generates an osteogenic environment to which mesenchymal stem cells respond and undergo osteogenic differentiation to form bone. Together with the osteogenic environment generated by the submicron surface structured calcium phosphate ceramic, icaritin enhanced the function of mesenchymal stem cells and bone formation was eventually enhanced.

Calvarial Defect Repair Evaluation

Studies have shown that angiogenesis plays a vital role in bone tissue repair process, and enhanced neovascularization accelerates bone formation (Karageorgiou and Kaplan, 2005; Oates et al., 2007; Barralet et al., 2009). As observed in **Figure 5**, an increase in blood vessels amount was seen from M0 to M250, the pores of all implants were occupied by soft tissues including blood vessels, indicating enhanced bone formation was associated with higher density of blood vessels. It has been shown that stem cells could reach to the osteoinductive calcium phosphate ceramic via blood circulation (Song et al., 2013). It is likely that icaritin first enhanced angiogenesis from which stem cells responsible for inductive bone formation could be recruited. When the stem cells were differentiated by CaP ceramic, icaritin enhanced the function of such differentiated cells to form bone.

It is thus worthy of performing studies to test the functionality of icaritin-containing osteoinductive CaP ceramic in bone regeneration in orthopedic sites. The *in vivo* bone regeneration effect of samples was evaluated by micro-CT and histological analysis. The 3D images of Micro-CT reconstruction in **Figure 7A** demonstrate newly formed bone within implants at week 4, 8, and 12, and the quantitative data of new bone volume (BV/TV) within the implants was measured by the 2D radiographs. Compared with M0 group, there was a significant

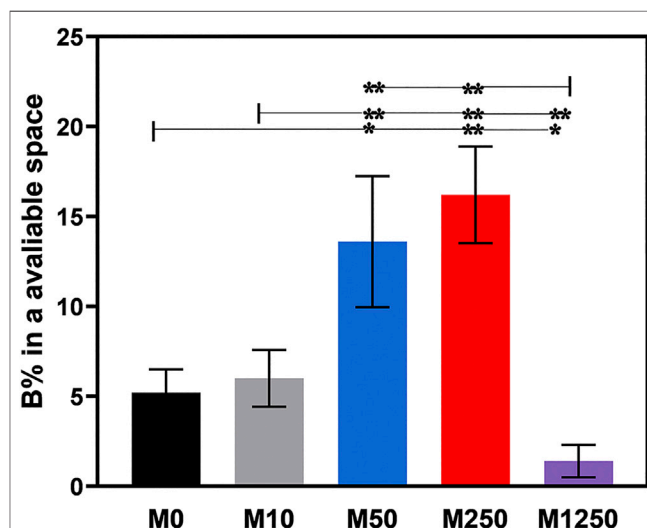


FIGURE 6 | Bone formation in the available space (%) of samples harvested from dogs (statistically significant differences are marked by * $p < 0.05$, ** $p < 0.01$).

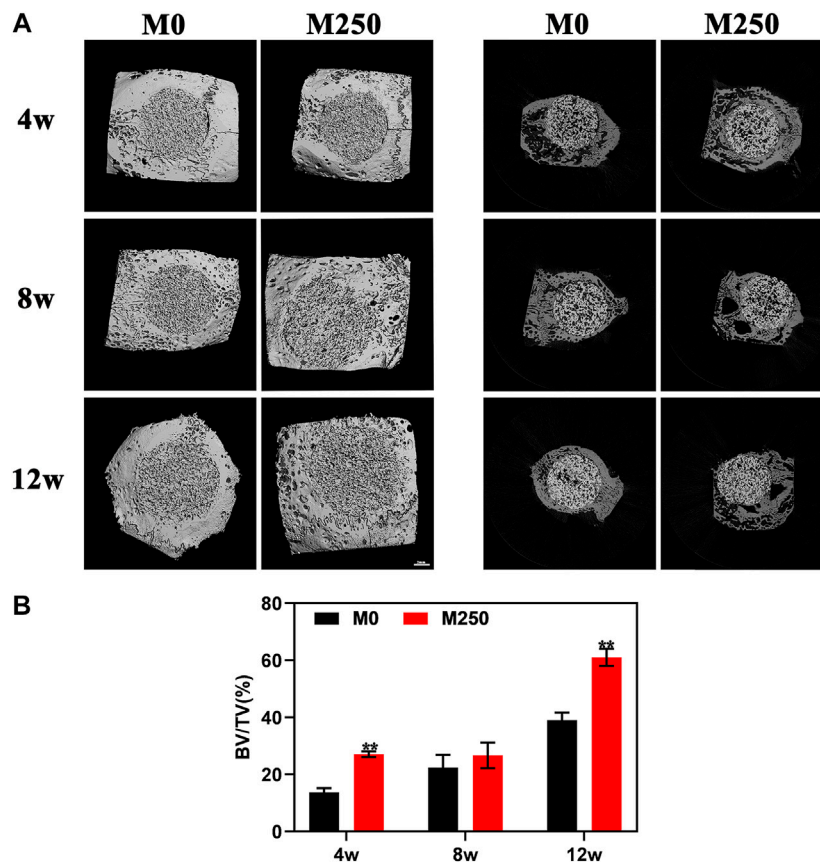


FIGURE 7 | Micro-CT analysis of M0, M1250 after calvarial implantation for 4, 8, and 12 weeks. **(A)** The corresponding three-dimensional reconstruction images of micro-CT results and representative axial sections. **(B)** Calculated bone volume/tissue volume (BV/TV) (Statistically significant differences are marked by * $p < 0.05$, ** $p < 0.01$).

increase in BV/TV in M250 group at week 4 (**Figure 7B**) ($p < 0.01$, $n = 3$). After 8 weeks post implantation, although the growth rate of the M250 group is lower than that of M0 group, the BV/TV of the M250 group is still higher than that of M0 group (**Figure 7B**). At week 12, the BV/TV in M250 group was significantly higher than that of M0 group (**Figure 7B**) ($p < 0.01$, $n = 3$). And the BV/TV of all groups at week 12 was higher than that of week 8.

Figures 8 and **10** display the histological manifestations in methylene blue and basic fuchsin stains after implantation for 4, 8 and 12 weeks, respectively. Observed from the axial and sagittal direction, the newly formed bone tissue became evident at week 4 with limited bony bridging along the radial border of the bone defect (**Figure 8A**, **Figure 8a₂**, **Figure 8B**, **Figure 8b₂**, **Figure 10A**, **Figure 10a₁**, **Figure 10a₂**, **Figure 10B**, **Figure 10b₁**, **Figure 10b₂**). Compared with week 4, at week 8, more new bone tissue in both groups grew into the scaffold, along the radial direction (**Figure 8C**, **Figure 8D**, **Figure 10C**, **Figure 10D**). Obviously, at week 12, the new bone tissue of the M250 group have almost penetrated the entire material (**Figure 8F**, **Figure 10F**). Serial graphs reveal how new bone first originates at the

resident bone edges from where it proceeds first along the external margins of the scaffold implant and then towards the center of the scaffold. Quantitative analysis (**Figure 9**) shows that at week 4, week 8 and week 12, the M250 group had more new bone in the defect compared to the M0 group. At week 4 and week 8, both groups had isolated new bone islands along the radial margins and within the pores of the scaffolds (**Figure 8a₁**, **Figure 8b₁**, **Figure 8c₁**, **Figure 8d₁**). The newly formed bone within the scaffold was seen to have remodelled towards mature lamellar bone with osteocytes within lacunae embedded in the bone matrix.

Newly formed vessels within the scaffold pores became visible in first 4 weeks in both groups (**Figures 11A,B**), and decreased from the next 4 weeks (**Figures 11C,D,G-I**). Quantitatively, compared with the M0 scaffold groups, the M250 scaffold group showed many more new vessels in terms of vessel volume, VEGF and FGF expression within bone defects at week 4, week 8 and week 12 ($n = 3$, **Figures 11G-I**).

Animal experiments results showed that icaritin significantly improve the ingrowth of blood vessel with a large amount of bone tissue penetrated the entire scaffold at

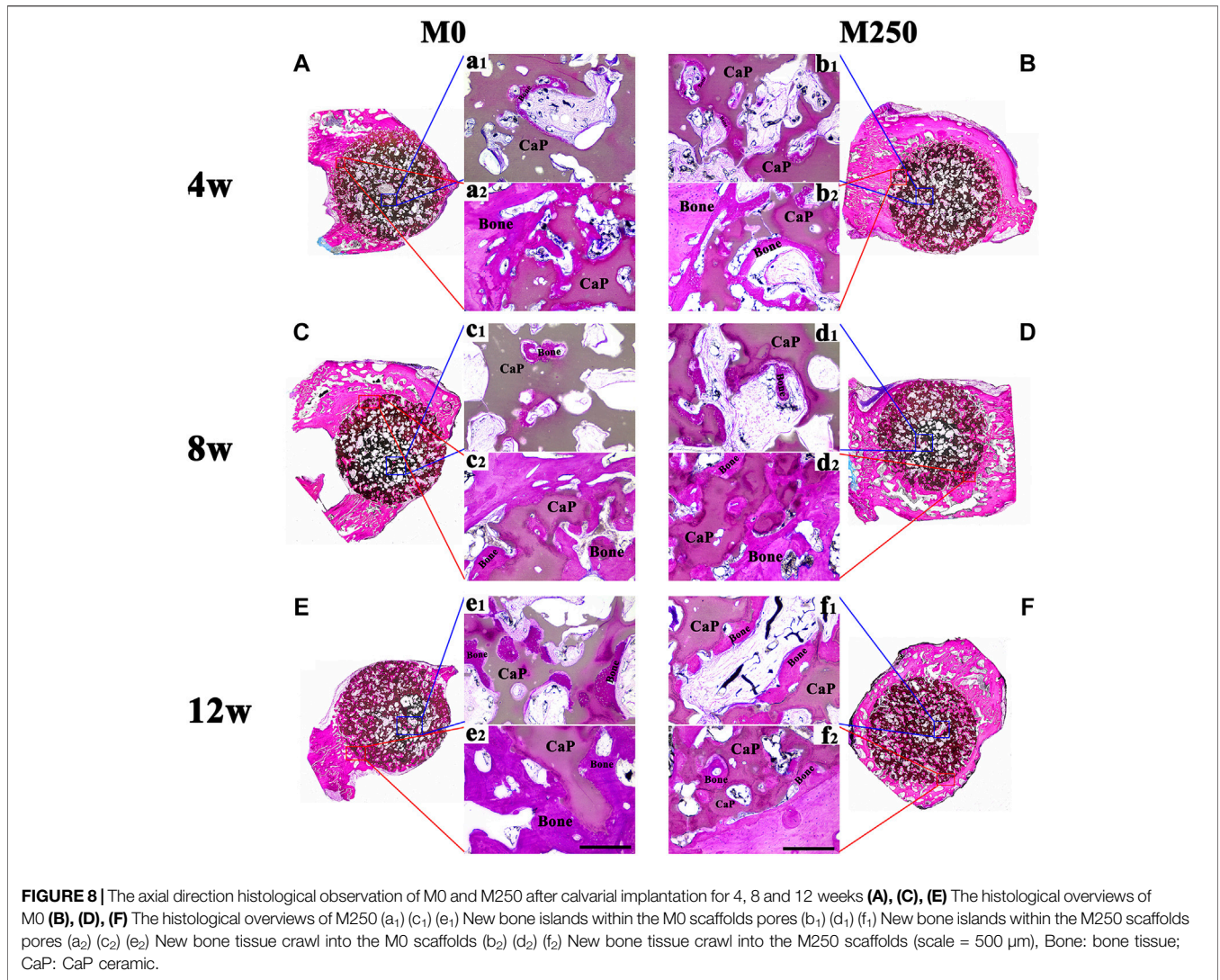


FIGURE 8 | The axial direction histological observation of M0 and M250 after calvarial implantation for 4, 8 and 12 weeks (A), (C), (E) The histological overviews of M0 (B), (D), (F) The histological overviews of M250 (a₁) (c₁) (e₁) New bone islands within the M0 scaffolds pores (b₁) (d₁) (f₁) New bone islands within the M250 scaffolds pores (a₂) (c₂) (e₂) New bone tissue crawl into the M0 scaffolds (b₂) (d₂) (f₂) New bone tissue crawl into the M250 scaffolds (scale = 500 μm), Bone: bone tissue; CaP: CaP ceramic.

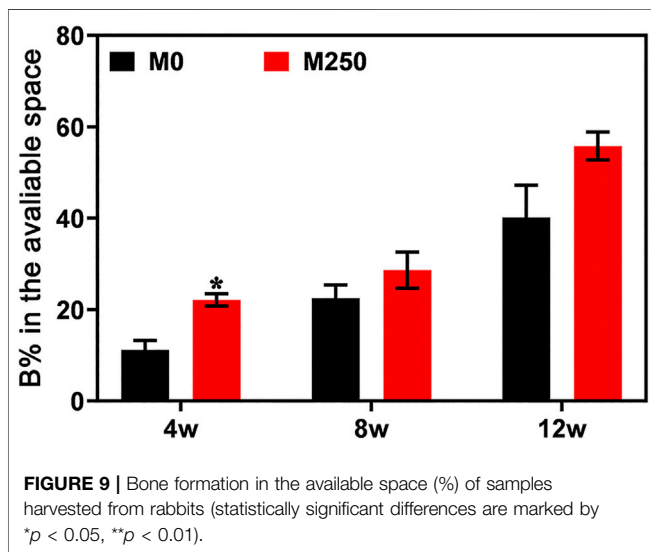


FIGURE 9 | Bone formation in the available space (%) of samples harvested from rabbits (statistically significant differences are marked by * $p < 0.05$, ** $p < 0.01$).

week 12, when compared with M0 group (Figures 7–10). And compared with week 4, although the number of blood vessels in M250 decreased at week 8, the number of connected blood vessels increased, accompanied by more bone regeneration (Figure 11). At week 12, the blood vessel volume of the M250 group was still higher than that of the M0 group (Figures 11E–I). These results support other evidence that icaritin enhanced angiogenesis and bone formation in rabbits when icaritin was incorporated into PLGA/TCP composites (Chen et al., 2012; Chen et al., 2013), indicating a possible link between angiogenesis and bone formation which was described in the phenomenon of osteoinduction caused by icaritin-loaded CaP ceramic.

CONCLUSION

When loaded into submicron surface structured CaP ceramics, icaritin was chemically retained and released

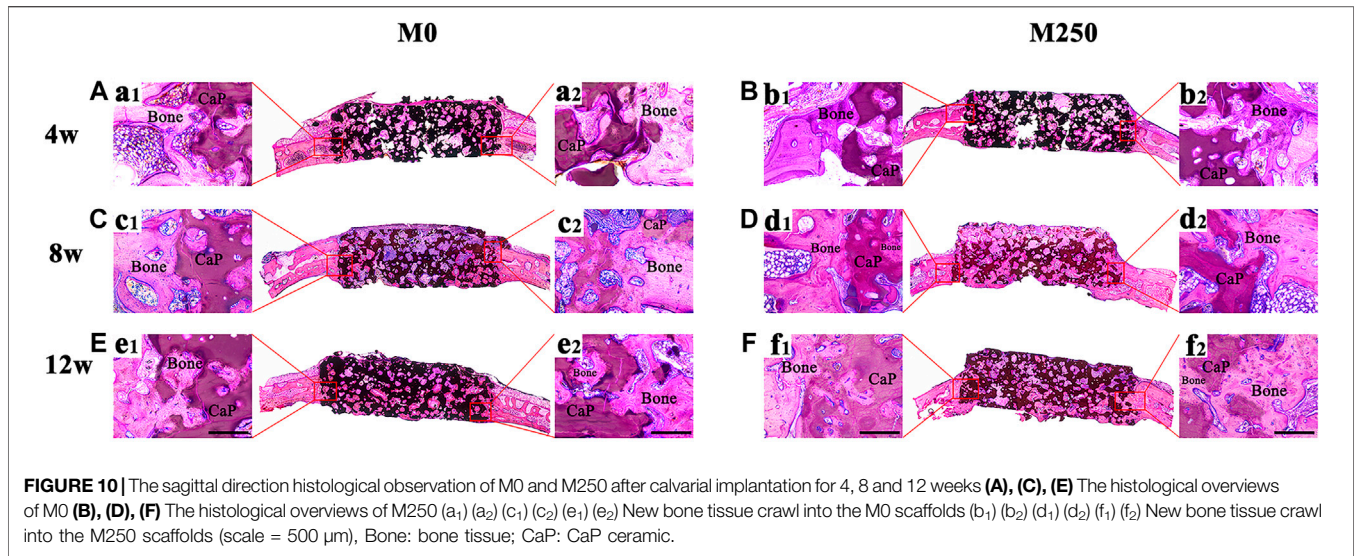


FIGURE 10 | The sagittal direction histological observation of M0 and M250 after calvarial implantation for 4, 8 and 12 weeks (A), (C), (E) The histological overviews of M0 (B), (D), (F) The histological overviews of M250 (a₁) (a₂) (c₁) (c₂) (e₁) (e₂) New bone tissue crawl into the M0 scaffolds (b₁) (b₂) (d₁) (d₂) (f₁) (f₂) New bone tissue crawl into the M250 scaffolds (scale = 500 μm), Bone: bone tissue; CaP: CaP ceramic.

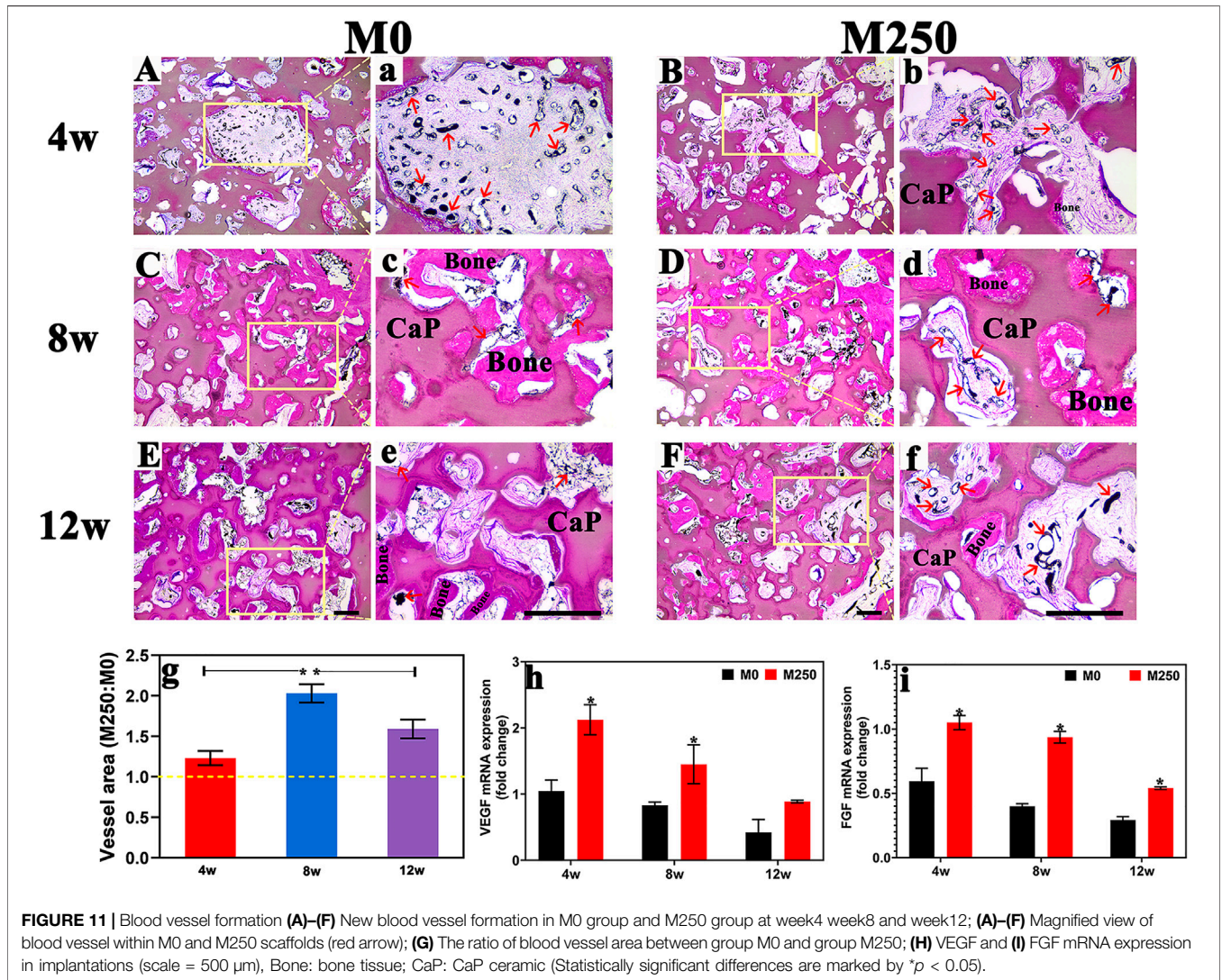


FIGURE 11 | Blood vessel formation (A)–(F) New blood vessel formation in M0 group and M250 group at week4 week8 and week12; (A)–(F) Magnified view of blood vessel within M0 and M250 scaffolds (red arrow); (G) The ratio of blood vessel area between group M0 and group M250; (H) VEGF and (I) FGF mRNA expression in implantations (scale = 500 μm), Bone: bone tissue; CaP: CaP ceramic (Statistically significant differences are marked by **p* < 0.05).

dose-dependently. With its release, icaritin enhanced osteogenesis of bone marrow stromal cells *in vitro* with the presence of osteogenic factors and enhanced bone formation initiated by submicron surface structured CaP ceramic in intramuscular implantation. Due to enhanced bone formation by icaritin, icaritin-containing osteoinductive CaP ceramic scaffolds presented the desired osteogenic and angiogenic potential, as evidenced in a rabbit calvarial defect model. The combination of icaritin and submicron surface structured CaP ceramics could thus be a novel strategy for bone regeneration.

DATA AVAILABILITY STATEMENT

The raw data supporting the conclusions of this article will be made available by the authors, without undue reservation.

REFERENCES

- Barralet, J., Gbureck, U., Habibovic, P., Vorndran, E., Gerard, C., and Doillon, C. J. (2009). Angiogenesis in calcium phosphate scaffolds by inorganic copper ion release. *Tissue Eng.* 15 (7), 1601–1609. doi:10.1089/ten.tea.2007.0370
- Bohner, M., Galea, L., and Doebelin, N. (2012). Calcium phosphate bone graft substitutes: failures and hopes. *J. Eur. Ceram. Soc.* 32 (11), 2663–2671. doi:10.1016/j.jeurceramsoc.2012.02.028
- Chai, Y. C., Kerckhofs, G., Roberts, S. J., Van Bael, S., Schepers, E., Vleugels, J., et al. (2012). Ectopic bone formation by 3D porous calcium phosphate-Ti6Al4V hybrids produced by perfusion electrodeposition. *Biomaterials* 33 (16), 4044–4058. doi:10.1016/j.biomaterials.2012.02.026
- Chen, S. H., Wang, X. L., Xie, X. H., Zheng, L. Z., Yao, D., Wang, D. P., et al. (2012). Comparative study of osteogenic potential of a composite scaffold incorporating either endogenous bone morphogenetic protein-2 or exogenous phytomolecule icaritin: an *in vitro* efficacy study. *Acta Biomater.* 8 (8), 3128–3137. doi:10.1016/j.actbio.2012.04.030
- Chen, S. H., Lei, M., Xie, X. H., Zheng, L. Z., Yao, D., and Wang, X. L. (2013). PLGA/TCP composite scaffold incorporating bioactive phytomolecule icaritin for enhancement of bone defect repair in rabbits. *Acta Biomater.* 9 (5), 6711–6722. doi:10.1016/j.actbio.2013.01.024
- Damien, C. J., and Parsons, J. R. (1991). Bone graft and bone graft substitutes: a review of current technology and applications. *J. Appl. Biomater.* 2 (3), 187–208. doi:10.1002/jab.770020307
- Davison, N. L., Gamblin, A. L., Layrolle, P., Yuan, H., de Bruijn, J. D., and Barrère-de Groot, F. (2014a). Liposomal clodronate inhibition of osteoclastogenesis and osteoinduction by submicrostructured beta-tricalcium phosphate. *Biomaterials* 35(19), 5088–5097. doi:10.1016/j.biomaterials.2014.03.013
- Davison, N. L., Luo, X., Schoenmaker, T., Everts, V., Yuan, H., Barrère-de Groot, F., et al. (2014b). Submicron-scale surface architecture of tricalcium phosphate directs osteogenesis *in vitro* and *in vivo*. *Eur. Cell. Mater.* 27, 281–287. doi:10.22203/ecm.v027a20
- Galia, E., Nicolaidis, E., Hörter, D., Löbenberg, R., Reppas, C., and Dressman, J. B. (1998). Evaluation of various dissolution media for predicting *in vivo* performance of class I and II drugs. *Pharm. Res. (N. Y.)* 15 (5), 698–705. doi:10.1023/a:1011910801212
- Habibovic, P., van der Valk, C. M., van Blitterswijk, C. A., De Groot, K., and Meijer, G. (2004). Influence of octacalcium phosphate coating on osteoinductive properties of biomaterials. *J. Mater. Sci. Mater. Med.* 15 (4), 373–380. doi:10.1023/b:jmsm.0000021104.42685.9f
- Hench, L. L., and Wilson, J. (1984). Surface-active biomaterials. *Science* 226 (4675), 630–636. doi:10.1126/science.6093253
- Huang, J., Yuan, L., Wang, X., Zhang, T. L., and Wang, K. (2007). Icaritin and its glycosides enhance osteoblastic, but suppress osteoclastic, differentiation and activity *in vitro*. *Life Sci.* 81 (10), 832–840. doi:10.1016/j.lfs.2007.07.015
- Huskens, J., and Sherry, A. D. (1998). Co-ordination chemistry and molecular mechanics study of the magnesium(II) and calcium(II) complexes of trisubstituted 1,4,7-triazacyclononane derivatives. *J. Chem. Soc. Dalton Trans.* 5 (1), 177–184. doi:10.1039/a703640j
- Ji, M., Chen, H., Yan, Y., Ding, Z., Ren, H., and Zhong, Y. (2020). Effects of tricalcium silicate/sodium alginate/calcium sulfate hemihydrate composite cements on osteogenic performances *in vitro* and *in vivo*. *J. Biomater. Appl.* 34 (10), 1422–1436. doi:10.1177/0885328220907784
- Karageorgiou, V., and Kaplan, D. (2005). Porosity of 3D biomaterial scaffolds and osteogenesis. *Biomaterials* 26 (27), 5474–5491. doi:10.1016/j.biomaterials.2005.02.002
- Lai, X., Ye, Y., Sun, C., Huang, X., Tang, X., Zeng, X., et al. (2013). Icaritin exhibits anti-inflammatory effects in the mouse peritoneal macrophages and peritonitis model. *Int. Immunopharm.* 16 (1), 41–49. doi:10.1016/j.intimp.2013.03.025
- Lee, K. G., Lee, K. S., Kang, Y. J., Hwang, J. H., Lee, S. H., Park, S. H., et al. (2018). Rabbit calvarial defect model for customized 3D-printed bone grafts. *Tissue Eng. C Methods.* 24 (5), 255–262. doi:10.1089/ten.TEC.2017.0474
- Luo, X., Barbieri, D., Davison, N., Yan, Y., de Bruijn, J. D., and Yuan, H. (2014). Zinc in calcium phosphate mediates bone induction: *in vitro* and *in vivo* model. *Acta Biomater.* 10(1), 477–485. doi:10.1016/j.actbio.2013.10.011
- McMillan, A., Nguyen, M. K., Gonzalez-Fernandez, T., Ge, P., Yu, X., Murphy, W. L., et al. (2018). Dual non-viral gene delivery from microparticles within 3D high-density stem cell constructs for enhanced bone tissue engineering. *Biomaterials* 161, 240–255. doi:10.1016/j.biomaterials.2018.01.006
- Murr, L. E. (2019). Strategies for creating living, additively manufactured, open-cellular metal and alloy implants by promoting osseointegration, osteoinduction and vascularization: an overview. *J. Mater. Sci. Technol.* 35 (2), 231–241. doi:10.1016/j.jmst.2018.09.003
- Oates, M., Chen, R., Duncan, M., and Hunt, J. A. (2007). The angiogenic potential of three-dimensional open porous synthetic matrix materials. *Biomaterials* 28 (25), 3679–3686. doi:10.1016/j.biomaterials.2007.04.042
- Peng, S., Zhang, G., Zhang, B. T., Guo, B., He, Y., Bakker, A. J., et al. (2013). The beneficial effect of icaritin on osteoporotic bone is dependent on the treatment initiation timing in adult ovariectomized rats. *Bone* 55 (1), 230–240. doi:10.1016/j.bone.2013.02.012
- Qin, L., Zhang, G., Sheng, H., Wang, X. L., Wang, Y. X., Yeung, K. W., et al. (2008). Phytoestrogenic compounds for prevention of steroid-associated osteonecrosis. *J. Musculoskelet. Neuronal Interact.* 8 (1), 18–21. doi:10.1007/978-3-540-45456-4_38
- Song, G., Habibovic, P., Bao, C., Hu, J., van Blitterswijk, C. A., Yuan, H., et al. (2013). The homing of bone marrow MSCs to non-osseous sites for ectopic bone formation induced by osteoinductive calcium phosphate. *Biomaterials* 34 (9), 2167–2176. doi:10.1016/j.biomaterials.2012.12.010
- van Dijk, L. A., Duan, R., Luo, X., Barbieri, D., Pelletier, M., Christou, C., et al. (2018). Biphasic calcium phosphate with submicron surface topography in an

ETHICS STATEMENT

The animal study was reviewed and approved by The First Affiliated Hospital of Chongqing Medical University.

AUTHOR CONTRIBUTIONS

HP and JL performed the experiments, analyzed and interpreted the results. YX performed the animal experiments. GL acquired the research operating funding, advised on the conception and conduction of the experiments and data analysis.

ACKNOWLEDGMENTS

The authors thank Science and Technology Project of Sichuan Province (2018FZ0108) for providing funding for this research.

- Ovine model of instrumented posterolateral spinal fusion. *JOR Spine*. 1 (4), e1039. doi:10.1002/jsp2.1039
- Xu, S., Lin, K., Wang, Z., Chang, J., Wang, L., Lu, J., et al. (2008). Reconstruction of calvarial defect of rabbits using porous calcium silicate bioactive ceramics. *Biomaterials* 29 (17), 2588–2596. doi:10.1016/j.biomaterials.2008.03.013
- Yao, D., Xie, X. H., Wang, X. L., Wan, C., Lee, Y. W., and Chen, S. H. (2012). Icaritin, an exogenous phytomolecule, enhances osteogenesis but not angiogenesis—an *in vitro* efficacy study. *PLoS One*. 7 (8), e41264. doi:10.1371/journal.pone.0041264
- Yuan, H., van Blitterswijk, C. A., de Groot, K., and de Bruijn, J. D. (2006). A comparison of bone formation in biphasic calcium phosphate (BCP) and hydroxyapatite (HA) implanted in muscle and bone of dogs at different time periods. *J. Biomed. Mater. Res.* 78 (1), 139–147. doi:10.1002/jbm.a.30707
- Yuan, H., Fernandes, H., Habibovic, P., de Boer, J., Barradas, A. M., and de Ruiter, A. (2010). Osteoinductive ceramics as a synthetic alternative to autologous bone grafting. *Proc. Natl. Acad. Sci. U.S.A.* 107 (31), 13614–13619. doi:10.1073/pnas.1003600107
- Zhang, G., Qin, L., and Shi, Y. (2007). Epimedium-derived phytoestrogen flavonoids exert beneficial effect on preventing bone loss in late postmenopausal women: a 24-month randomized, double-blind and placebo-controlled trial. *J. Bone Miner. Res.* 22 (7), 1072–1079. doi:10.1359/jbmr.070405
- Zhang, G., Pan, X. H., Xie, X. H., He, B. Y., Li, G., Leung, K. S., et al. (2008). Icaritin, a potential estrogen receptor beta antagonist molecule Icaritin, promote osteoporotic fracture repair in ovariectomized mice: preliminary finding at 3 weeks post fracture. *Bone* 43 (Suppl. S1), S76–S77. doi:10.1016/j.bone.2008.07.081
- Zhang, G., Qin, L., Sheng, H., Wang, X. L., Wang, Y. X., and Yeung, D. K. (2009). A novel semisynthesized small molecule icaritin reduces incidence of steroid-associated osteonecrosis with inhibition of both thrombosis and lipid-deposition in a dose-dependent manner. *Bone* 44 (2), 345–356. doi:10.1016/j.bone.2008.10.035
- Zhang, J., Luo, X., Barbieri, D., Barradas, A. M., de Bruijn, J. D., and van Blitterswijk, C. A. (2014). The size of surface microstructures as an osteogenic factor in calcium phosphate ceramics. *Acta Biomater.* 10 (7), 3254–3263. doi:10.1016/j.actbio.2014.03.021
- Zhang, J., Barbieri, D., ten Hoopen, H., de Bruijn, J. D., van Blitterswijk, C. A., and Yuan, H. (2015). Microporous calcium phosphate ceramics driving osteogenesis through surface architecture. *J. Biomed. Mater. Res.* 103 (3), 1188–1199. doi:10.1002/jbm.a.35272

Conflict of Interest: The authors declare that the research was conducted in the absence of any commercial or financial relationships that could be construed as a potential conflict of interest.

Copyright © 2020 Peng, Li, Xu and Lv. This is an open-access article distributed under the terms of the Creative Commons Attribution License (CC BY). The use, distribution or reproduction in other forums is permitted, provided the original author(s) and the copyright owner(s) are credited and that the original publication in this journal is cited, in accordance with accepted academic practice. No use, distribution or reproduction is permitted which does not comply with these terms.